Cycle-frequency content EEG analysis improves the assessment of respiratory-related cortical activity

Xavier Navarro-Sune[1], Mathieu Raux[1,2], Anna L. Hudson[1,3,4] ,Thomas Similowski[1,2], Mario Chavez[5]

1. Sorbonne Université, INSERM UMRS1158 Neurophysiologie Respiratoire Expérimentale et Clinique, Hôpital Pitié-Salpêtrière. F-75005, Paris, France.
2. AP-HP, Groupe Hospitalier APHP-Sorbonne Université, Hôpital Pitié-Salpêtrière, Département R3S, F-75013, Paris, France
3. College of Medicine and Public Health, Flinders University, 5042, Adelaide, Australia
4. Neuroscience Research Australia and University of New South Wales, 2031, Sydney, Australia
5. CNRS UMR 7225, Hôpital Pitié-Salpêtrière. F-75005, Paris, France.

Keywords: Event-related spectral perturbation, Time-frequency analysis, Electroencephalography, Event-related potentials, Respiratory-related cortical activity

Abstract

Time-Frequency (T-F) analysis of EEG is a common technique to characterise spectral changes in neural activity. This study explores the limitations of utilizing conventional spectral techniques in examining cyclic event-related cortical activities due to challenges, including high inter-trial variability. Introducing the Cycle-Frequency (C-F) analysis, we aim to enhance the evaluation of cycle-locked respiratory events. For synthetic EEG that mimicked cycle-locked pre-motor activity, C-F had better frequency and time precision compared to conventional T-F analysis, even when the number of trials was reduced from 50 to 20. Preliminary validations using EEG data during both unloaded breathing and loaded breathing (that evokes pre-motor activity) suggest potential benefits of using the C-F method, particularly in normalizing time units to cyclic activity phases and refining baseline placement and duration. The proposed approach could provide new insights for the study of rhythmic neural activities, complementing T-F analysis.

INTRODUCTION

Breathing is the only vital function controlled both automatically and voluntarily (Horn & Waldrop, 1998; Mohammadshirazi et al., 2023). The involvement of the brain in breathing control ranges from increased attentional resources (Moore et al., 2012), to voluntary modification of the breathing pattern (Pouget et al., 2018), as well as compensatory mechanisms in the presence of ventilatory constraints that hinder adequate airflow (Raux et al., 2007). A respiratory-related cortical activation has been described in various respiratory disorders, including chronic obstructive pulmonary disease (COPD) (Nguyen et al., 2018), obstructive sleep apnea (Launois et al., 2015), congenital central alveolar hypoventilation (Tremoureux et al., 2014) and respiratory muscle weakness (Georges et al., 2016). In this context, cortical activation is interpreted as a compensatory mechanism, and is often associated with dyspnea (defined as an upsetting or distressing awareness of breathing activity) (Manning & Mahler, 2001).

The preparation and execution of breathing movements involve specific brain areas, and both the frequency content and latencies of respiratory-related premotor and motor potentials depend on various scenarios. The generation of slow cortical (readiness) potentials in the primary motor cortex and supplementary motor area is typically observed during the preparation of self-paced breaths (Hudson et al., 2018; Macefield & Gandevia, 1991). Slow potentials occur 1.5 to 1 s before the onset of inspiration and are currently studied using averaging techniques on event-related electroencephalographic (EEG) segments (Raux et al., 2007). Pre- and post-stimuli changes in EEG activity of faster rhythms may also be present in the sensorimotor cortex. The most studied frequencies in this case are the *alpha* (8-12Hz) and *beta* (13-30Hz) bands (Pfurtscheller & Lopes da Silva, 1999), with a specific interval between 9 and 13 Hz, referred to as the *mu* rhythm, which is considered particularly insightful as it provides understanding into the neural mechanisms underlying the interaction between action and perception (Hari, 2006). Our previous investigations of respiratory-related changes in these faster rhythms had varied results (Dubois et al 2016 and Hudson et al 2016)

Changes in EEG frequencies during sensory stimulation were first quantified using the method of event-related spectral desynchronization (ERD) (Pfurtscheller, 1977). The term desynchronization, which describes an event-related decrease in activity, was later complemented with the opposite effect, that is, an event-related power increase, to describe EEG changes under the term event-related desynchronization/synchronization (ERDS) (Pfurtscheller, 1992). This technique relies on averaging a number of EEG segments, time-

locked to an event (trials), and measuring amplitude changes in both the temporal and spectral domains, with respect to a reference period of a few seconds before the event occurs (baseline) (Pfurtscheller & Lopes da Silva, 1999). By time-frequency (T-F) transformations of the EEG signals, event-related changes can be represented in a spectrogram, a 2D representation that allows localization of the time-frequency components. This technique is commonly referred to as event-related spectral perturbation (ERSP) (Makeig et al., 2004).

At present, ERSP is the most employed representation in computational neurosciences, as it allows for easy visualization of power spectral changes induced or evoked by events related to both external (visual, auditory, tactile) and internal (self-paced movement) stimuli. Current protocols typically define a fixed value of latencies and duration for each stimulus to facilitate data segmentation into trials and analyses. However, in case of self-initiated or self-paced stimuli, the interpretation of ERSP can be biased by inter-trial variability, which refers to different trial segments' duration mainly due to fatigue or uncontrolled cognitive processes of the subject during the experiment (Fox et al., 2007; Provost et al., 2018). Although some strategies can minimize this variability (e.g. discarding short trials), the conventional procedure for computing ERSP is rarely questioned.

Several alternatives to the standard procedure have been proposed to improve the ERSP estimation. Lemm and colleagues (Lemm et al., 2009) introduced a new computational approach that measures ERSP using a dynamic reference, which considers the dynamics of unperturbed EEG rhythms instead of a constant baseline level, resulting in more accurate estimations of the evoked somatosensory activity. Another study reported that optimal ERSP detection depends on the identification of participant-specific reactive bands, and used a band-limited multiple Fourier linear combiner to demonstrate that the classification performance of cue-based motor imagery tasks was significantly better than that of conventional ERSP estimation (Wang et al., 2012). While both methods can be useful in reducing bias in ERSP estimation under external stimuli, addressing the variability of trials related to endogenous (self-initiated), unbalanced stimuli remains a challenge for motor imagery tasks (Daeglau et al., 2020) and gait studies (Delval et al., 2020). To the best of our knowledge, the relevance of conventional ERSP for the particular case of respiratory-related cortical activity has not yet been addressed.

Breathing is controlled by automatic central pattern generators located in the brainstem and by and voluntary control pathways, both of which are in constant interaction during wakefulness (Laviolette et al., 2013; Straus et al., 2004). This can lead to high inter-trial variability in terms

of segment duration and neural dynamics under certain conditions (Datta et al., 1991; Homma & Masaoka, 2008). Therefore, conventional event-related spectral analysis may not be accurate in identifying respiratory-related evoked potentials.

In this paper, we will first discuss the standard methodology used to compute ERSPs and its limitations when it comes to the specificity of experiments assessing respiratory-related cortical activity. Here we introduce the cycle-frequency (C-F) transformation, a new approach that considers the cyclic nature of breathing to improve the estimation of ERSP. This new method will be validated using a model that generates respiratory-related potentials in an EEG-like signal. Finally, we will test the cycle-frequency transformation on real EEG data, comparing and discussing the benefits and limitations of this new representation.

METHODS

Conventional procedure to obtain ERSPs

As for most experimental paradigms in cognitive neuroscience, the study of spectral disturbances related to respiratory events can be studied with conventional time-frequency representations. The usual procedure for obtaining these time-frequency maps (Bullock, 1992) can be summarized as follows: (i) the EEG signal is divided into n excerpts $\boldsymbol{x} = \{x_1, x_2, \dots, x_n\}$, of l seconds (m samples) around the events of interest; (ii) each EEG segment is transformed into the time-frequency domain, producing a complex variable $\boldsymbol{X} = \{X_1, X_2, \dots, X_n\}$ with $X_i \in \mathbb{C}^{m \times q}$, where q denotes the number of frequencies; (iii) the absolute values of X_i are averaged to obtain a single image representing the power of induced activity, $\overline{X^P}$, whereas the complex values of X_i are used to compute the phase alignment between trials, often referred as intertrial coherence, $\overline{X^I}$; (iv) finally, average maps are normalized with respect to a baseline period. Evoked activities can be similarly obtained by averaging time-frequency transformation X_i of all epochs, and by taking the absolute value of the final map.

To identify the regions with relevant power changes, statistical significance can be assessed by cluster-based permutation tests (Bullock, 1992) or bootstrapping (Gross et al., 2013). However, statistical tests are performed on grand-average maps, which are obtained by averaging an ensemble of maps from individual participants. The results of standard ERSP analysis strongly depend on the choice of:

1. The length of the segments (l), which is fixed according to the experimental conditions. The segments are centered around the event of interest (t_0 = 0 s) and divided into a pre-

event period (t_{pre}) and a post-event period (t_{post}). The length of each period should be chosen to capture the potentials of interest while avoiding overlap with neighboring trials.

2. The baseline period, which should be distant from the onset of the potentials of interest to ensure a good contrast. Typically, it is a time interval extending up to 20-25% of t_{pre} or t_{post}, depending on the study (Picton et al., 2000). Various techniques can be used to correct by the baseline, but in general, the activity of the normalized maps is reported as the average power per frequency of this period. These changes in T-F are represented as percentage, standard deviation, or decibels.

Although the conventional procedure to obtain ERSPs can be useful for the estimation of respiratory-related potentials under ventilatory constraints (Dubois et al., 2016; Hudson et al., 2016) it has significant limitations due to the inter-trial variability caused by different duration length of respiratory cycles (see Figure 1). Indeed, the resting respiratory activity in humans is characterized by its breath-by-breath variability (van den Bosch et al., 2021), which stems from the intrinsic complexity of brainstem automatic neural command (Mangin et al., 2008) and from suprapontine perturbations. This variability pertains to tidal volume (the volume inhaled during a single breath), the respiratory cycle period, the duration of inspiration, and the duration of expiration (Fiamma et al., 2007). It can result in coefficients of variation between 15 and 40% for these variables (Fiamma et al., 2007), which limits the use of time-frequency maps.

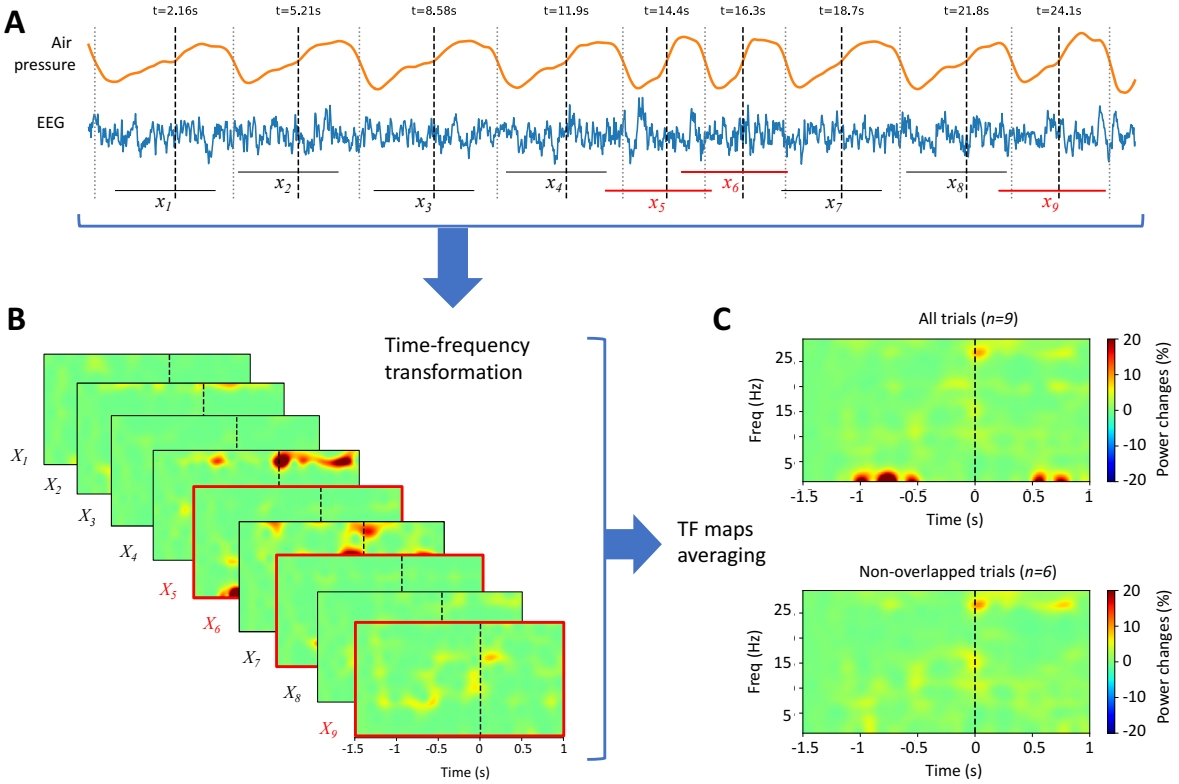

Figure 1: Illustration of the conventional procedure for computing ERSPs to study pre-inspiratory potentials using EEG recorded during spontaneous breathing. A: The EEG signal is divided into nine trials (x_1 to x_9) according to the onset of inspiration (black vertical dashed lines), and pre-inspiratory and post-inspiratory times (in this example t_{pre}=-1.5s and t_{post}=1s). The onset of expiration is marked with grey vertical dotted lines and trials with significant overlap (i.e. when the next trial commences prior to 90% completion of the current trial) are highlighted in red. B: For each trial, time-frequency transformation (using complex Morlet wavelet) and baseline correction (between -1.5 and -1.25 s) are performed, resulting in n=9 time-frequency maps (X_1 to X_9). C: The average power maps are obtained by averaging all trials (upper map) or using only non-overlapping trials (lower map).

Alternative procedure to obtain ERSPs

The hypothesis of cycle-dependent potentials

Several studies suggest that respiratory-related potentials may be dependent on the phase of the breathing cycle. For instance, Davenport et al (1986) found that the latencies of respiratory-related somatosensory evoked potentials depend on the intensity of the underlying neural drive to breathe, and hypothesized that somatosensory potentials induced by loaded breathing are

delayed in comparison to analogous evoked potentials for electrically evoked somatosensory potentials, due to the time required for the stimulus to activate sufficient inspiratory afferents to evoke a response (Davenport et al., 1986). A recent study demonstrated that intracortical EEG and the breathing signal are significantly synchronized during volitional breathing by using spectral coherence techniques (Herrero et al., 2018; Watanabe et al., 2023).

Based on these studies, we hypothesize that breathing potentials, which typically exhibit a non-regular cyclic pattern, should be considered "cycle-locked" rather than time-locked potentials. Regarding the reference event (inspiration), pre- and post-inspiratory potentials can be distinguished. Although they may have different implications for the processing of somatosensory or (pre-)motor information, we will refer to them as inspiratory potentials for simplicity. This assumption has two practical implications for our analysis: i) inspiratory potentials start at a specific phase of the breathing cycle; hence their latencies are jittered in time according to the cycle duration and; ii) inspiratory potentials are active during a specific phase interval, and their duration is proportional to the cycle length.

To represent ERSPs using the phase of the respiratory cycle rather than time, we propose to construct cycle-frequency maps. To do so, we require an adaptive segmentation of the EEG according to breathing cycles using respiratory marks. We approximate each breath as a whole cycle (2π radians) between two consecutive marks that delimit a complete breath. If inspiratory marks are used, then expiration is assumed to occur in the middle of the period (phase of the cycle, $\varphi = \pi$ rad).

To segment the EEG, we need first to define the analysis phase interval $[\phi_s, \phi_e]$, with bounds denoting the start and end phase. If the study concerns pre-inspiratory potentials, the interval could include half of the previous breath (i.e. from the expiration onset at $\phi_s =$ -π rad) and a portion of the inspiration (e.g. $\phi_e = \pi/2$ rad). Similar to T-F analysis, the events of interest (inspiration marks) are placed at $\phi = 0$. Importantly, cycle-based approach systematically avoids the inclusion of the previous inspiration $\phi <$ -π rad, which also contains pre-inspiratory potentials, ensuring thus correct baseline placement. The baseline can be established by selecting the 15-20% leftmost portion of the pre-inspiratory time (see Figure 2). If the analysis

concerns post-inspiratory potentials, then the phase interval can be modified to center the window to the activity of interest.

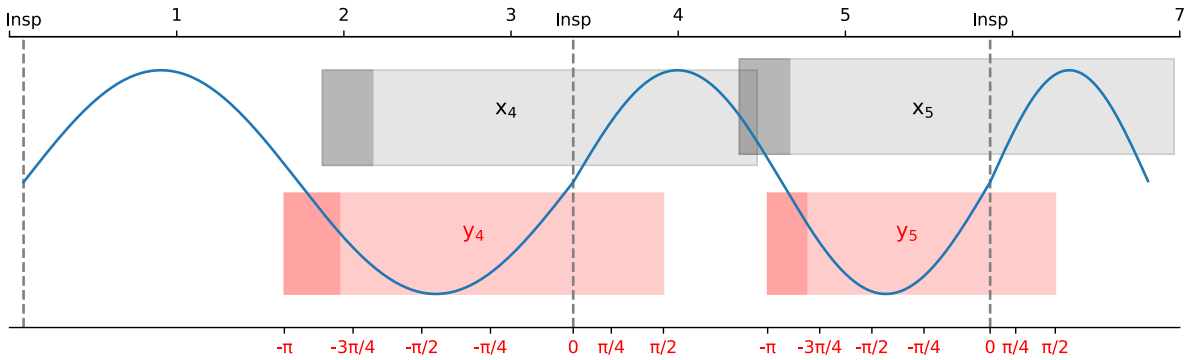

Figure 2: Illustration of two segmentations adapted to cycles of different duration. The breathing trace is approximated by a quasi-sinusoidal period between consecutive inspiratory marks. Grey upper rectangles correspond to conventional trials (x_4 and x_5) of equal length (l_4=l_5=2.5s), with fixed baselines (dark grey areas). Red rectangles correspond to cycle-segmented trials (y_4 and y_5) of variable length with a phase interval [-π, π/2] rad. Dark red areas correspond to the baseline periods adapted to each cycle by taking the 20% of the pre-inspiratory time, equivalent to the phase interval $\left[-\pi, -\frac{4\pi}{5}\right]$.

Construction of cycle-frequency maps

To construct cycle-frequency maps, we start by adaptively segmenting EEG as described above. Cycle-based segmentation yields *n* segments, denoted as $y = \{y, y_2, \dots, y_n\}$, with y_i of variable length l_i in seconds, $(i = 1,2, \dots n)$ containing a number of samples $m_i = l_i f_s$, with f_s denoting the sampling frequency. We denote the shortest and longest breaths by l_{min} and l_{max}, respectively.

The next step is to compute the T-F representation on ***y***, choosing the optimal transformation parameters. As mentioned earlier, there are multiple decomposition approaches, but the most common is based on the continuous wavelet transform (Cohen, 2014). This T-F representation convolves the EEG signal with a set of complex Morlet wavelets, defined as complex sine waves tapered by a Gaussian (Tallon-Baudry & Bertrand, 1999) as follows:

$$w(t, f) = e^{\frac{-t^2}{2\sigma^2}} e^{2i\pi f t}$$

where *i* is the imaginary unit given by $\sqrt{-1}$ and $\sigma = \eta/2\pi f$ is the width of the Gaussian. The parameter η, also referred as to the number of cycles, determines the time-frequency precision

trade-off. A smaller η results in better temporal resolution but lower frequency resolution, whereas a larger η results in better frequency resolution but lower temporal resolution. Although η can be constant, in neural time-series it is recommended to use a variable number of cycles as a function of frequency, starting from a few cycles for the lowest frequency and increasing up to several cycles for the highest frequency of interest (Cohen, 2014).

The choice of parameters for computing the T-F representation includes the boundary frequencies represented in the spectrograms (f_{min} and f_{max}), and the frequency bin (f_b), which define the number of frequencies (q). The choice of f_{min} is generally determined by the shortest trial. Following the recommendations (Cohen, 2014), at least three complete oscillations of the lowest frequency to be analyzed should be contained in the signal. Therefore, we set $f_{min} \geq 3/l_{min}$. On the other hand, the highest frequency is limited only by the Nyquist frequency, hence $f_{max} \leq f_s/2$ even if, in practice, f_{max} can be set to a much lower value, where most relevant information in EEG is contained.

The time-frequency transformation of $\boldsymbol{y}$ will produce the corresponding spectrograms, $\boldsymbol{Y'} = \{Y'_1, Y'_2, \dots, Y'_n\}$, with $Y'_i \in \mathbb{C}^{m_i \times q}$, where m_i denotes the number of samples of trial i. Next, $\boldsymbol{Y'}$ is converted from time to cycle domain to obtain $\boldsymbol{Y} = \{Y_1, Y_2, \dots, Y_n\}$, with $Y_i \in \mathbb{C}^{p \times q}$. The number of phase values (bins), p, must satisfy the condition $p \geq \frac{2f_{max}}{l_{min}}$ to ensure the correct representation of the highest frequencies. Likewise, the phase interval of interest $\Delta\phi = \phi_e - \phi_s$ have to be taken into consideration. For instance, given a set of T-F maps with l_{min} = 1.5 s, f_{max}=30 Hz and $\Delta\phi = {}^{3\pi}/_{2}$ rads (or 270°), choosing a phase bin $r_\phi = {}^{\pi}/_{90}$ rads (or 2°) results in $p = \Delta\phi / r_\phi = 135$, which satisfies the condition $p \geq \frac{2f_{max}}{l_{min}} = 20$.

Once the value of p is properly selected, the conversion from time to cycle domain can be achieved by downsampling by a trial-dependent factor, $k_i = \frac{p}{m_i}$. To minimise the aliasing effect of downsampling, we employed here a poliphase filter (Hsiao, 1987). Finally, a baseline correction is applied by averaging Y_i to obtain the power, $\overline{\boldsymbol{Y^P}}$, and to compute inter-trial phase coherence from the complex values Y_i

RESULTS

To validate the proposed method, we first used artificial EEG signals containing cycle-locked activity of known frequency and amplitude, specifically designed to study pre-inspiratory potentials. Then, we applied the conventional and the cycle-frequency procedure to obtain

ERSP and compared them. Subsequently, we tested both methods on real EEG data obtained from a healthy volunteer breathing under different respiratory conditions.

Tests on synthetic data

We generated artificial EEG signals using two distinct generative models: the first model incorporates pre-inspiratory activity in accordance with the hypothesis of cycle-locked potentials while the second model generates time-locked potentials to inspiratory marks. In both models, artificial EEG was generated by combining background activity based on random noise with superimposed sinusoidal bursts. These bursts mimic synchronization of EEG activity seen with movement.

For the cycle-locked model, the onset of each burst was determined by the phase of the cycle (set to $\phi_p^{ini} = -\pi/2$), and its duration was proportional to the cycle length (burst phase interval, $\Delta\phi_p = \pi/4$). For the time-locked model, the onset latency of oscillations was within the typical range of 300 to 700 milliseconds prior to trigger marks (Kilavik et al., 2013) and their duration was arbitrarily set to half the value of the latency.

The frequency of the sinusoidal bursts (f_p) was set to 20 Hz for both models, a value typically found in pre-motor activity (Kilavik et al., 2013). Bursts were tapered by a Hanning window of the same duration to smooth the edges. The background noise follows a Gaussian distribution rescaled by a factor of 10^{-5}, and the sinusoidal bursts peak was set to 5 μV. Given the targeted activity, the frequencies of interest for time-frequency transformations were f_{min}=5 and f_{max}=30 Hz with steps of 0.5 Hz, hence $q=50$.

To better "mimic" respiratory event-related EEG epochs, we generated pseudo-inspiratory marks according to typical human breathing rhythms (ranging from 2 to 6 seconds per breath) as follows: each cycle duration was determined by adding a normally distributed random number with zero mean and unit variance to an average cycle duration of 4 seconds. If this addition resulted in a time less than the minimum cycle duration of 2 seconds, then the absolute value of the negative random number was added instead. Using this approach, we created synthetic EEG at f_s=500 Hz simulating breathing constraints that induced pre-inspiratory potentials cycle-locked and time-locked to the inspiration marks, with a mean respiratory period, $\overline{T}$, of 4 s.

To compare conventional time-frequency to cycle-frequency representations, we obtained three sets of segments for each one of the generative models :

1) $\boldsymbol{x}$ was the result of performing conventional fixed length segmentation, $l=2$ s (t_{pre}=-1.5 s ; t_{post}=0.5 s). The number of samples per trial, m, was 1000.
2) $\boldsymbol{y}$ was composed of mean-adapted segments, i.e. excerpts segmented according to the mean duration of breaths (4s). The phase span was $\frac{3}{2}\pi$ radians with $\phi_i = -\pi$ and $\phi_e = \frac{\pi}{4}$ but segments had fixed length, $l=3$ s (t_{pre}=-2 s ; t_{post}=1 s) and m=1500.
3) z was composed by cycle-adapted segments, with l_i depending of the duration of each breath. The phase span was $\frac{3}{2}\pi$ radians with $\phi_i = -\pi$ and $\phi_e = \frac{\pi}{4}$.

The time-frequency transformation was performed using Morlet wavelets of increasing η with frequency. Thus, the frequencies of the wavelets ranged from 2.5 Hz to 14.75 Hz in 50 frequency bins. This resulted in $\boldsymbol{X}$, with $\boldsymbol{X_i} \in \mathbb{C}^{\mathbf{1000\times 50}}$. For cycle-frequency maps, a phase bin $r_\phi = 1°$ (with a p=270) satisfied the restriction imposed by l_{min}=2 s and f_{max} = 30 Hz. Therefore, the cycle-frequency transformation of $\boldsymbol{y}$ and z resulted, respectively, in $\boldsymbol{Y}$ and $\boldsymbol{Z}$, with $\{\boldsymbol{Y_i}, \boldsymbol{Z_i}\} \in \mathbb{C}^{\mathbf{270\times 50}}$. All power maps were baseline-corrected the leftmost 15% of samples to visualize power ratio changes. Additionally, we conducted simulations with n=50 and n=20 trials to assess the robustness of T-F and C-F techniques in the context of limited data availability. All computations were performed using Python 3.7 language with MNE package (Gramfort et al., 2013).

Data generated using the cycle-locked and time-locked models are denoted, respectively, with superscripts (1) and (2). Figure 3 shows time- and cycle-frequency transformations of artifical data generated by the cycle-locked model. As shown, cycle-locked potentials appeared around 20Hz, but with varying power values and time precision. In $\mathbf{Z}^{(1)}$ (cycle-frequency transformation of cycle-adapted segments), bursts (i.e. EEG synchronisation) were more noticeable and well identified in phase, whereas their temporal localization in $\boldsymbol{X}^{(1)}$ (conventional time-frequency transformation of fixed-length segments) spaned over 0.5 seconds and the borders were not well-defined. We also observed that using a segmentation based in the mean

duration of breaths ($\boldsymbol{Y}^{(1)}$) can identify the cycle-locked potentials, although with lower power values and precision compared to $\boldsymbol{Z}^{(1)}$.

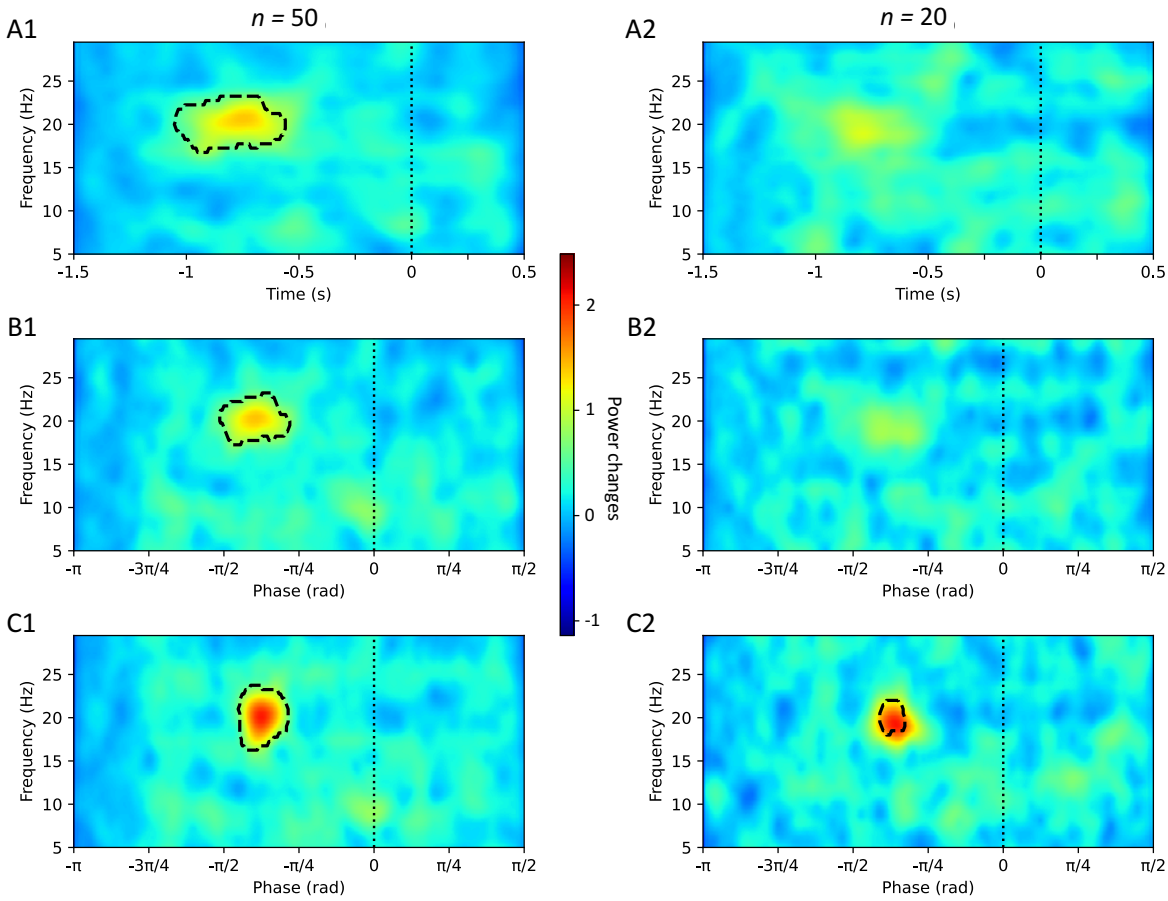

Figure 3: Cycle-frequency maps derived from synthetic EEG generated by the cycle-locked model. Panels A1, B1 and C1 illustrate different power representations: A1 shows the conventional time-frequency map of fixed-length segments ($\boldsymbol{X}^{(1)}$). B1 presents the cycle-frequency map employing segments with a fixed duration based on the mean respiratory rate ($\boldsymbol{Y}^{(1)}$). C1 displays the cycle-frequency map using cycle-adapted segmentation ($\boldsymbol{Z}^{(1)}$). Left plots (A1, B1, C1) depict results from n=50 simulted trials, while right plots (A2, B2, C2) show equivalent representations from another simulation with n=20 trials. The color scale expresses the ratio of power changes with respect to the baseline. Black dotted lines enclose statistically significant areas found by the permutation test.

To statistically quantify these observed differences, we conducted standard permutation tests to compare the significance of pre-inspiratory activity against the baseline period. Tests involved 1000 permutations and a significance level of 0.05 with threshold-free cluster

enhancement (Smith & Nichols, 2009). Permutation tests confirmed that only power maps obtained from the set $\boldsymbol{Z}^{(1)}$ retained significance and precision in terms of potential localizationwhen the number of averaged trials decreased from *n*=50 to *n*=20 (see Figure 3C2). As expected, the in-phase alignment of cycle-locked activities maximized the signal-to-noise ratio.

Figure 4 illustrates time- and cycle-frequency transformations of artifical data generated by the time-locked model. Conventional time-frequency transformations effectively detected time-locked potentials, with statistically significant regions aligning with the latencies and frequency of the bursts, observerd consistently across simulations with n=50 and n=20 trials (panels A1 and A2). However, cycle-frequency maps using segmentation based on the mean duration of breaths ($\boldsymbol{Y}^{(2)}$) revealed reduced significant areas corresponding to the bursts due to time-to-cycle conversion losses, as evident in panels B1 and B2.

Finally, using cycle-frequency transformation of cycle-adapted segments ($\boldsymbol{Z}^{(2)}$), statistically significant activity around the burst was observed only in simulations with n=50 trials (panel C1). In contrast, with only n=20 trials, a small non-significant area proximal to the burst was visible in panel C2, potentially confounded with other areas containing spurious activity.

Regarding the two representation techniques examined, conventional time-frequency representations can detect cycle-locked activity and, cycle-frequency representations can detect time-locked activity particularly when a sufficient number of trials provide a fair signal-to-noise ratio. However, when signal-to-noie ratios are lower (n<=20 trials), conventional time-frequency representations may fail to accurately identify phase-locked activity. Similarly, for a

reduced number of trial, cycle-frequency representation limits the identification of time-locked activity.

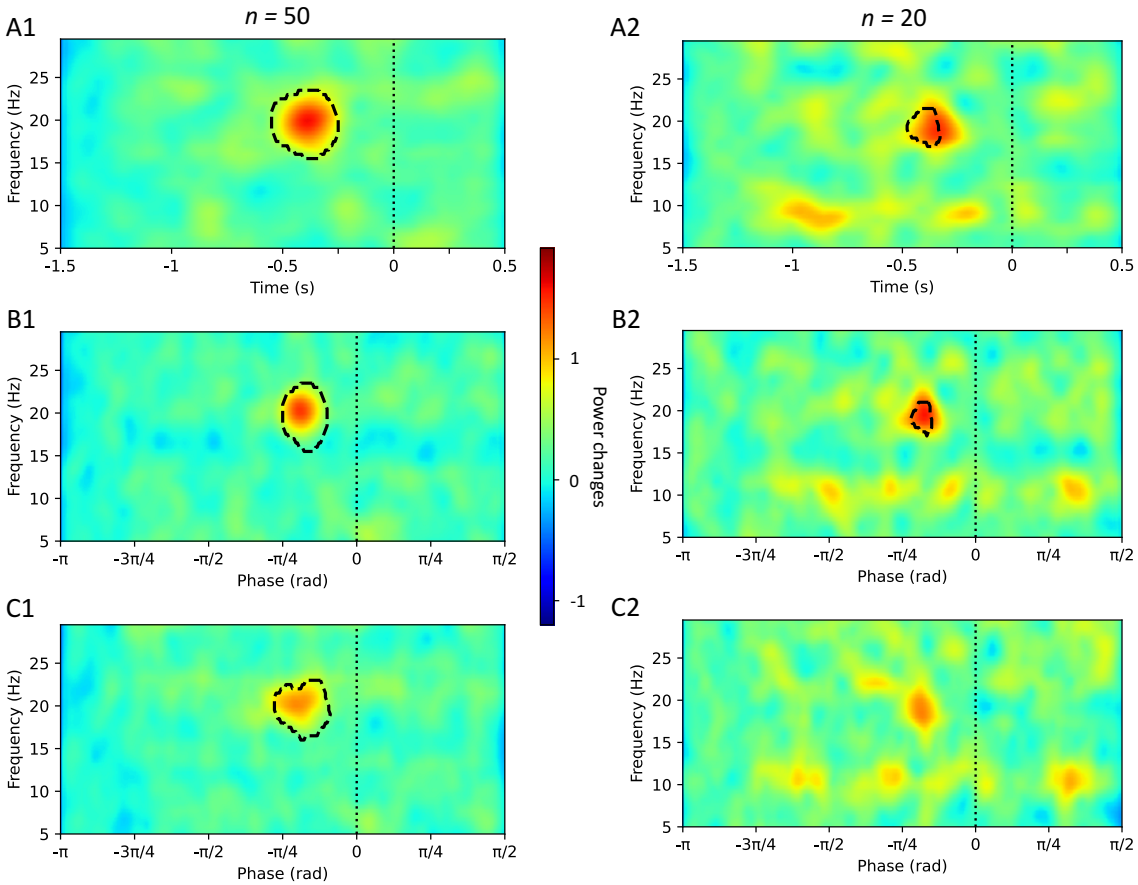

Figure 4: Cycle-frequency maps derived from synthetic EEG generated by the time-locked model. Panels A1, B1 and C1 illustrate different power representations: A1 shows the conventional time-frequency map of fixed-length segments ($\boldsymbol{X}^{(2)}$). B1 presents the cycle-frequency map employing segments with a fixed duration based on the mean respiratory rate ($\boldsymbol{Y}^{(2)}$). C1 displays the cycle-frequency map using cycle-adapted segmentation ($\boldsymbol{Z}^{(2)}$). Left plots (A1, B1, C1) depict results from n=50 simulted trials, while right plots (A2, B2, C2) show equivalent representations from another simulation with n=20 trials. The color scale expresses the ratio of power changes with respect to the baseline. Black dotted lines enclose statistically significant areas found by the permutation test.

Tests on real data

To illustrate the potential of our proposal, we compared qualitatively, standard Time-Frequency (T-F) and Cycle-Frequency (C-F) maps using real data acquired from a 32-channel EEG system following the International 10-20 System. The dataset, as presented in (Hudson 2022), consists of data from 25 healthy subjects who breathed through a mouthpiece under two distinct conditions: unloaded breathing (UB) and loaded breathing (LB). In the LB condition, subjects experienced increased effort to maintain adequate airflow due to the application of an inspiratory threshold load, whereas in UB, subjects breathed normally. In LB, we expect pre- and post-inspiratory potentials to arise not only due to ventilatory compensation (pre-motor and motor activity) but also due to the unpleasant sensations associated with breathing difficulty (somatosensory activity).

For illustration purposes, we selected the subject with the fastest breathing rate in UB, T_{QB} = 2.72 ± 0.47 s (mean respiratory period ± standard deviation) to maximize the number of overlapped trials. Following the standard fixed segmentation parameters (t_{pre} = -1.5 s; t_{post} = 0.5 s), overlap occurred when breathing periods were under 2.5 s, which was the case for 54 out of a total of 220 segments. In LB, respiratory periods significantly increased, T_{LB} = 8.73 ± 2.01 s, resulting in only n = 66 available trials.

Time-frequency and cycle-frequency analyses were conducted using the same parameters as for synthetic signals. After obtaining different maps for each channel, we computed an average map covering the pre-motor area (average of positions F3, Fz, F4, FC1, and FC2) and an average map covering somatosensory positions (average of C3, Cz, C4, CP1, and CP2) to investigate differences between the three techniques. These areas are of particular interest in the analysis of respiratory-related potentials as they reflect the preparation of breaths and the sensory perception of breathing.

In UB, pre-motor area maps exhibit minimal pre- and post-inspiratory potentials within the *mu* band (9-13 Hz), and distinctions between the three techniques—conventional T-F maps, C-F maps utilizing mean-adapted segments, and CF maps utilizing cycle-adapted segments—are almost negligible (see left column in Figure 5). In the somatosensory area (right column in Figure 4), increased activity within the same frequency band is noticeable, with latencies spanning both before and after the inspiratory trigger (approximately from -0.5 to 0.5 s and from -π/4 to π/2). Respiratory-related somatosensory activity in T-F and C-F maps follows a similar pattern; however, power changes in the latter are slightly enhanced, likely due to better

alignment of potentials across trials. The permutation test did not find statistically significant changes with respect to the baseline period.

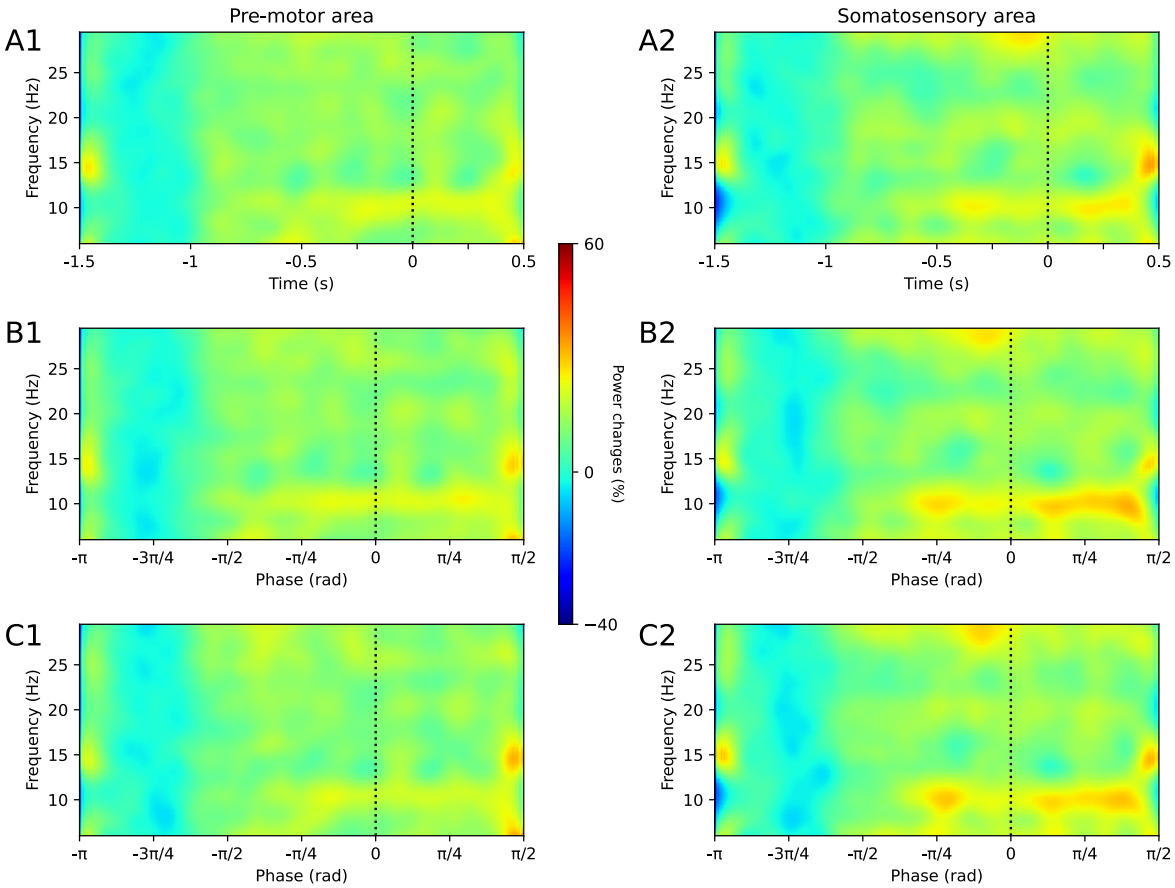

Figure 5: Power maps obtained from real EEG during unloaded breathing (n=166 trials). The left column (A1, B1, C1) displays average maps using electrodes in the pre-motor area, while the right column (A2, B2, C2) presents average maps from the somatosensory area (see Results for EEG positions). The top row (A1, A2) illustrates conventional time-frequency maps using fixed segmentation ([-1.5; 0.5] sec); the middle row (B1, B2) showcases cycle-frequency maps with fixed segmentation based on the average breathing period; and the bottom row (C1, C2) displays cycle-frequency maps with cycle-adaptive segmentation.

In LB, due to the constraints on breathing, there is a more pronounced presence of respiratory-related cortical activity compared to the UB condition. Regarding pre-motor activity, T-F maps suggest a light and brief beta increase (specifically between 15 and 25 Hz, as shown in Figure 5-A1) beginning approximately 1 second before inspiration. Lower-frequency activations (ranging from 6 to 12 Hz) accompany the beta increase, occurring both before and after inspiration. In the somatosensory area, pre-inspiratory changes are observed close to the

inspiratory trigger, spanning from 8 to 25 Hz, while post-inspiratory potentials manifest in both low and high-frequency (>20 Hz) ranges.

Given the longer duration of breathing cycles in the loaded condition, C-F maps display an extended temporal window, causing the potentials to appear compressed compared to their counterparts in T-F maps. Beyond the visual effect, longer segments in the cycle-frequency transformation can yield unrealistic values for the onset and duration of respiratory-related potentials. For instance, if we consider that pre-inspiratory potentials start at phase –π/4, the corresponding time for a long breath of T=15 s (t_{pre}=-7.5 s; t_{post}= 3.25 s) is -1.875 seconds. Although this latency might be plausible according to prior research on slow pre-inspiratory cortical potentials (Hudson et al., 2018; Macefield & Gandevia, 1991; Raux et al., 2007), it is unrealistic for faster activity such as the mu rhythm (Kilavik et al., 2013; Pfurtscheller & Lopes da Silva, 1999). To address this issue, we propose to apply an arbitrary threshold during segmentation. In the LB condition analysed here, we set $t_{pre}^{max} = 2T_{QB}$= 5.44 seconds.

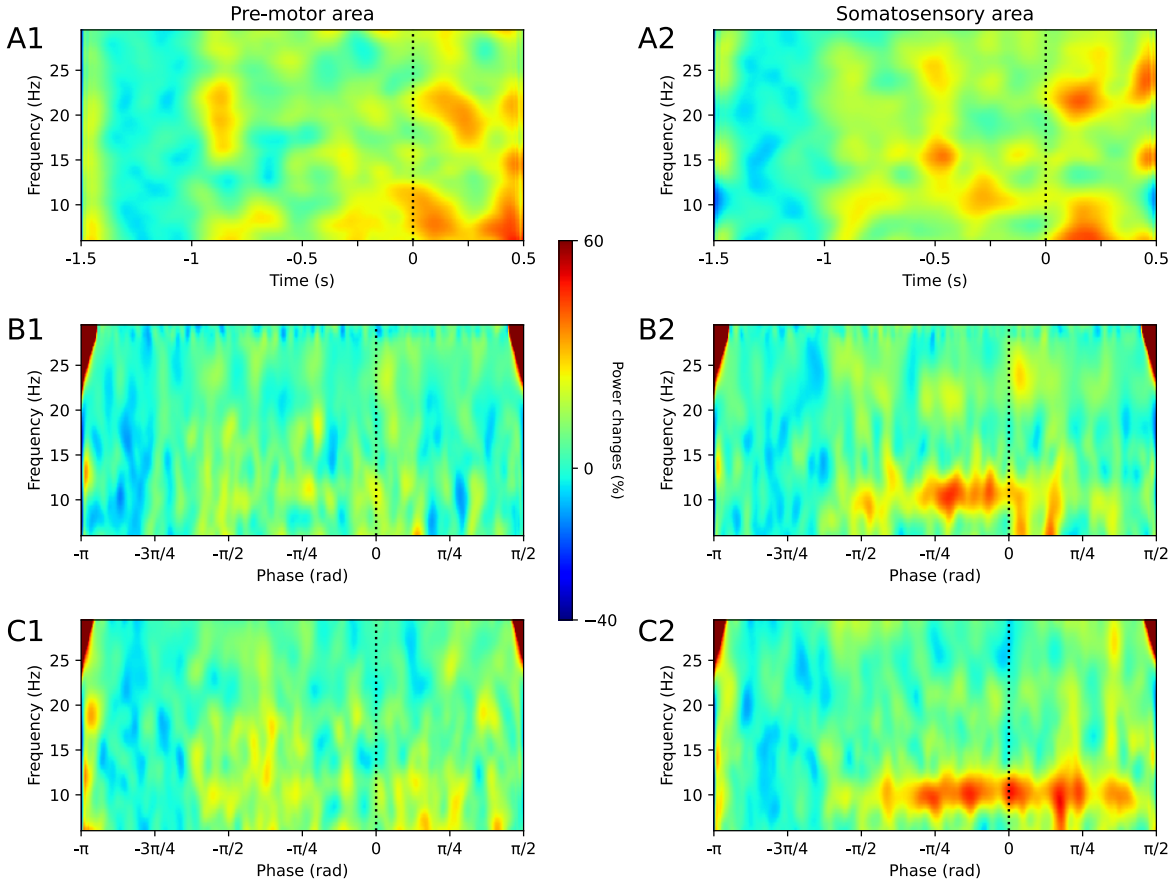

Figure 6: Power Maps Derived from Real EEG during loaded breathing (n=66 trials). The left column (A1, B1, C1) displays average maps utilizing electrodes in the pre-motor area, while the right

column (A2, B2, C2) presents average maps from the somatosensory area. The first row (A1, A2) illustrates conventional time-frequency maps employing fixed segmentation ([-1.5 ; 0.5] sec); the second row (B1, B2) showcases cycle-frequency maps with fixed segmentation based on the average breathing period; and the third column (C1, C2) exhibits cycle-frequency maps utilizing cycle-adaptive segmentation.

Following this criterion, we obtained C-F maps depicted in the second and third rows of Figure 6. In the pre-motor area, no clear changes appear during the respiratory cycle. In contrast, power changes can be clearly observed in the somatosensory area within the 8 to 12 Hz range, spanning both before and after inspiration. This clearly suggests that cycle-based analysis could be a better approach to study cyclic respiratory related cortical activities.

DISCUSSION

In this study, we introduced a new procedure for analyzing event-related spectral perturbation, called cycle-frequency (C-F) transformation, specifically designed to examine cycle-locked events by adjusting trial lengths to match the duration of each cycle. Non-strictly-periodic EEG activities are prevalent in many paradigms. To address this variability, several studies have employed time-warping methods to enhance the characterization of temporal dynamics in neural activity. This technique, previously applied in analyses of self-paced rhythmic movements (Chemin et al., 2018) and gait analysis (Wagner et al., 2019), involves the contraction or dilation of temporal signals to align trial lengths with a specified mean period. The C-F transformation offers an alternative technique where trial segmentation is adapted to the duration of each breath.

We have demonstrated that, for the respiratory context, the use of C-F representation has several advantages over the conventional time-frequency (T-F) procedure. One of the advantages is the ability to normalize the time relative to the phase of the cyclic activity. As the duration of each breath may be highly variable (Fiamma et al., 2007), this normalization facilitates the averaging of trials and their comparison across different conditions and subjects. Another advantage is the possibility to set the latency and duration of the baseline adapted to the cycle length. This baseline placement strategy systematically avoids the overlap of the reference period with active periods of neighbouring events.

As a result, the analysis of respiratory-related cortical activity becomes more robust to inter-trail variability (due for instance to changing states during an experiment). Considering

interventions to relieve dyspnea in mechanically ventilated patients, breathing rates are likely to change substantially (Raux et al., 2019). Therefore, our proposal can provide, for example, a benchmark for comparing intervention-related cortical activities during fast and slow breathing.

To evaluate the effectiveness of C-F analysis, we used artificial signals mimicking cycle-locked and time-locked pre-inspiratory EEG potentials. Our findings demonstrate that C-F analysis enhances the detection of cycle-locked potentials compared to conventional T-F procedures, which may obscure cycle-locked activity due to temporal misalignment during the averaging process. Conversely, while time-locked acivity can be efectively detected by T-F maps, C-F analysis fails when signal-to-noise levels were lower (n=20 trials). Employing cycle-frequency maps with segments of fixed duration based on the mean respiratory rate may offer a compromise for detecting both time- and cycle-locked activities.

To illustrate our approach with real data, we applied both cycle-frequency and time-frequency analyses to EEG data from a single subject. Our new analysis method revealed respiratory-related activity that was not evident with the traditional method as shown here, and in our previous studies using time-frequency analyses of loaded breathing (Hudson et al., 2016) and hypocapnic breathing (Dubois et al., 2016). Although the frequency content and latencies observed matched typical changes underlying motor preparation tasks, these regions did not show statistical significance in the permutation test. Further research is needed then to confirm the extent to which time- and cycle-locked activities may cohexist within the same experimental condition. Nevertheless, the use of both T-F and C-F maps shows promise for studing the overall cortical activity related to breathing.

By analyzing real data we also conclude that fast cycle-locked potentials might not start with long latencies in very long cycles. While there is evidence that readiness potentials may commence, under certain conditions, as early as 2 seconds before the onset of the movement (Hudson et al., 2018; Macefield & Gandevia, 1991; Raux et al., 2007), such latency is unrealistic for faster rhythms. Therefore, we proposed implementing a threshold to restrict the maximum length of EEG segments to be converted into the cycle domain, thereby avoiding time compression that could blur fast transient activity. This threshold should be a reasonable value based on the available evidence, such as the upper quartile of breathing periods at rest or twice the mean period.

The proposed method presents some limitations that should be carefully considered. Since the downsampling of C-F maps leads to a lower temporal resolution of high frequencies, it is crucial

to intially evaluate whether parameters l_{min} and f_{max} accurately represent the desired frequencies. In datasets containing trials with significant variations in duration, it may be necessary to exclude the shortest trials to raise l_{min} and therefore increase f_{max}. We also notice that the downsampling procedure in the CF transformation may have an impact on the statitistical significance of permutation tests (reducing the number of pixels can dilute the power of specific, time-located activities). Similarly, the impact of cycle asymmetry (i.e. when the durations of inspiration and expiration differ significantly) needs further study.

Future works should explore the generalizability of C-F analysis to other types of self-paced responses to investigate the potential of this technique for the study of cycle-locked potentials. This research could have notable implications for the characterization of respiratory and limb movement disorders and lead to a better understanding of the neural control of rhythmic movements.

CONCLUSION

The objective of this paper is to introduce a new tool for computing event-related spectral perturbations in cortical activity associated with cycle or internal-paced movements. This tool is intended to be used in conjunction with conventional time-frequency (T-F) analysis rather than as a replacement, as time-locked potentials may coexist with cycle-locked potentials. Supplementary material in https://doi.org/10.17605/OSF.IO/ZM5UG includes the code and sample data to produce C-F maps to enable the reproduction of our results and facilitate further investigations.

REFERENCES

1. Bullock, T. H. (1992). Introduction to Induced Rhythms: A Widespread, Heterogeneous Class of Oscillations. In E. Başar & T. H. Bullock (Eds.), *Induced Rhythms in the Brain* (pp. 1–26). Birkhäuser. https://doi.org/10.1007/978-1-4757-1281-0_1

2. Chemin, B., Huang, G., Mulders, D., & Mouraux, A. (2018). EEG time-warping to study non-strictly-periodic EEG signals related to the production of rhythmic movements. *Journal of Neuroscience Methods*, *308*, 106–115. https://doi.org/10.1016/j.jneumeth.2018.07.016

3. Cohen, M. X. (2014). *Analyzing Neural Time Series Data: Theory and Practice*. MIT Press.

4. Daeglau, M., Zich, C., Emkes, R., Welzel, J., Debener, S., & Kranczioch, C. (2020). Investigating Priming Effects of Physical Practice on Motor Imagery-Induced Event-Related Desynchronization. *Frontiers in Psychology*, *11*.

https://www.frontiersin.org/articles/10.3389/fpsyg.2020.00057

5. Datta, A. K., Shea, S. A., Horner, R. L., & Guz, A. (1991). The influence of induced hypocapnia and sleep on the endogenous respiratory rhythm in humans. *The Journal of Physiology*, *440*(1), 17–33. https://doi.org/10.1113/jphysiol.1991.sp018693

6. Davenport, P. W., Friedman, W. A., Thompson, F. J., & Franzen, O. (1986). Respiratory-related cortical potentials evoked by inspiratory occlusion in humans. *Journal of Applied Physiology*. https://doi.org/10.1152/jappl.1986.60.6.1843

7. Delval, A., Bayot, M., Defebvre, L., & Dujardin, K. (2020). Cortical Oscillations during Gait: Wouldn't Walking Be So Automatic? *Brain Sciences*, *10*(2), Article 2. https://doi.org/10.3390/brainsci10020090

8. Dubois, M., Chenivesse, C., Raux, M., Morales-Robles, A., Nierat, M.-C., Garcia, G., Navarro-Sune, X., Chavez, M., Martinerie, J., & Similowski, T. (2016). Neurophysiological Evidence for a Cortical Contribution to the Wakefulness-Related Drive to Breathe Explaining Hypocapnia-Resistant Ventilation in Humans. *Journal of Neuroscience*, *36*(41), 10673–10682. https://doi.org/10.1523/JNEUROSCI.2376-16.2016

9. Fiamma, M.-N., Straus, C., Thibault, S., Wysocki, M., Baconnier, P., & Similowski, T. (2007). Effects of hypercapnia and hypocapnia on ventilatory variability and the chaotic dynamics of ventilatory flow in humans. *American Journal of Physiology - Regulatory, Integrative and Comparative Physiology*, *292*(5), R1985–R1993. https://doi.org/10.1152/ajpregu.00792.2006

10. Fox, M. D., Snyder, A. Z., Vincent, J. L., & Raichle, M. E. (2007). Intrinsic Fluctuations within Cortical Systems Account for Intertrial Variability in Human Behavior. *Neuron*, *56*(1), 171–184. https://doi.org/10.1016/j.neuron.2007.08.023

11. Georges, M., Moraviec, E., Raux, M., Gonzalez-Bermejo, J., Pradat, P.-F., Similowski, T., & Morélot-Panzini, C. (2016). Cortical drive to breathe in amyotrophic lateral sclerosis: A dyspnoea-worsening defence? *European Respiratory Journal*, *47*(6), 1818–1828. Scopus. https://doi.org/10.1183/13993003.01686-201

12. Gramfort, A., Luessi, M., Larson, E., Engemann, D., Strohmeier, D., Brodbeck, C., Goj, R., Jas, M., Brooks, T., Parkkonen, L., & Hämäläinen, M. (2013). MEG and EEG data analysis with MNE-Python. *Frontiers in Neuroscience*, *7*. https://www.frontiersin.org/articles/10.3389/fnins.2013.00267

13. Gross, J., Baillet, S., Barnes, G. R., Henson, R. N., Hillebrand, A., Jensen, O., Jerbi, K., Litvak, V., Maess, B., Oostenveld, R., Parkkonen, L., Taylor, J. R., van Wassenhove, V., Wibral, M., & Schoffelen, J.-M. (2013). Good practice for conducting and reporting MEG research. *NeuroImage*, *65*, 349–363. https://doi.org/10.1016/j.neuroimage.2012.10.001

14. Hari, R. (2006). Action–perception connection and the cortical mu rhythm. In C. Neuper & W. Klimesch (Eds.), *Progress in Brain Research* (Vol. 159, pp. 253–260). Elsevier. https://doi.org/10.1016/S0079-6123(06)59017-X

15. Herrero, J. L., Khuvis, S., Yeagle, E., Cerf, M., & Mehta, A. D. (2018). Breathing above the brain stem: Volitional control and attentional modulation in humans. *Journal of Neurophysiology*, *119*(1), 145–159. https://doi.org/10.1152/jn.00551.2017

16. Homma, I., & Masaoka, Y. (2008). Breathing rhythms and emotions. *Experimental Physiology*, *93*(9), 1011–

1021. https://doi.org/10.1113/expphysiol.2008.042424

17. Horn, E. M., & Waldrop, T. G. (1998). Suprapontine control of respiration. *Respiration Physiology*, *114*(3), 201–211. https://doi.org/10.1016/s0034-5687(98)00087-5

18. Hsiao, C.-C. (1987). Polyphase filter matrix for rational sampling rate conversions. *ICASSP '87. IEEE International Conference on Acoustics, Speech, and Signal Processing*, *12*, 2173–2176. https://doi.org/10.1109/ICASSP.1987.1169404

19. Hudson, A. L., Navarro-Sune, X., Martinerie, J., Pouget, P., Raux, M., Chavez, M., & Similowski, T. (2016). Electroencephalographic detection of respiratory-related cortical activity in humans: From event-related approaches to continuous connectivity evaluation. *Journal of Neurophysiology*, *115*(4), 2214–2223. https://doi.org/10.1152/jn.01058.2015

20. Hudson, A. L., Niérat, M.-C., Raux, M., & Similowski, T. (2018). The Relationship Between Respiratory-Related Premotor Potentials and Small Perturbations in Ventilation. *Frontiers in Physiology*, *9*. https://www.frontiersin.org/articles/10.3389/fphys.2018.00621

21. Kilavik, B. E., Zaepffel, M., Brovelli, A., MacKay, W. A., & Riehle, A. (2013). The ups and downs of beta oscillations in sensorimotor cortex. *Experimental Neurology*, *245*, 15–26. https://doi.org/10.1016/j.expneurol.2012.09.014

22. Launois, C., Attali, V., Georges, M., Raux, M., Morawiec, E., Rivals, I., Arnulf, I., & Similowski, T. (2015). Cortical Drive to Breathe during Wakefulness in Patients with Obstructive Sleep Apnea Syndrome. *Sleep*, *38*(11), 1743–1749. https://doi.org/10.5665/sleep.515

23. Laviolette, L., Niérat, M.-C., Hudson, A. L., Raux, M., Allard, E., & Similowski, T. (2013). The supplementary motor area exerts a tonic excitatory influence on corticospinal projections to phrenic motoneurons in awake humans. *PloS One*, *8*(4), e62258. https://doi.org/10.1371/journal.pone.0062258

24. Lemm, S., Müller, K.-R., & Curio, G. (2009). A Generalized Framework for Quantifying the Dynamics of EEG Event-Related Desynchronization. *PLOS Computational Biology*, *5*(8), e1000453. https://doi.org/10.1371/journal.pcbi.1000453

25. Macefield, G., & Gandevia, S. C. (1991). The cortical drive to human respiratory muscles in the awake state assessed by premotor cerebral potentials. *The Journal of Physiology*, *439*, 545–558. https://doi.org/10.1113/jphysiol.1991.sp018681

26. Makeig, S., Debener, S., Onton, J., & Delorme, A. (2004). Mining event-related brain dynamics. *Trends in Cognitive Sciences*, *8*(5), 204–210. https://doi.org/10.1016/j.tics.2004.03.008

27. Mangin, L., Fiamma, M.-N., Straus, C., Derenne, J.-P., Zelter, M., Clerici, C., & Similowski, T. (2008). Source of human ventilatory chaos: Lessons from switching controlled mechanical ventilation to inspiratory pressure support in critically ill patients. *Respiratory Physiology & Neurobiology*, *161*(2), 189–196. https://doi.org/10.1016/j.resp.2008.02.006

28. Manning, H. L., & Mahler, D. A. (2001). Pathophysiology of dyspnea. *Monaldi Archives for Chest Disease = Archivio Monaldi Per Le Malattie Del Torace*, *56*(4), 325–330.

29. Maris, E., & Oostenveld, R. (2007). Nonparametric statistical testing of EEG- and MEG-data. *Journal of Neuroscience Methods*, *164*(1), 177–190. https://doi.org/10.1016/j.jneumeth.2007.03.024

30. Mohammadshirazi, A., Apicella, R., Zylberberg, B. A., Mazzone, G. L., & Taccola, G. (2023). Suprapontine Structures Modulate Brainstem and Spinal Networks. *Cellular and Molecular Neurobiology*, *43*(6), 2831–2856. https://doi.org/10.1007/s10571-023-01321-z

31. Moore, A., Gruber, T., Derose, J., & Malinowski, P. (2012). Regular, brief mindfulness meditation practice improves electrophysiological markers of attentional control. *Frontiers in Human Neuroscience*, *6*. https://www.frontiersin.org/articles/10.3389/fnhum.2012.00018

32. Nguyen, D. A. T., Boswell-Ruys, C. L., McBain, R. A., Eckert, D. J., Gandevia, S. C., Butler, J. E., & Hudson, A. L. (2018). Inspiratory pre-motor potentials during quiet breathing in ageing and chronic obstructive pulmonary disease. *The Journal of Physiology*, *596*(24), 6173–6189. https://doi.org/10.1113/JP275764

33. Pfurtscheller, G. (1977). Graphical display and statistical evaluation of event-related desynchronization (ERD). *Electroencephalography and Clinical Neurophysiology*, *43*(5), 757–760. https://doi.org/10.1016/0013-4694(77)90092-x

34. Pfurtscheller, G. (1992). Event-related synchronization (ERS): An electrophysiological correlate of cortical areas at rest. *Electroencephalography and Clinical Neurophysiology*, *83*(1), 62–69. https://doi.org/10.1016/0013-4694(92)90133-3

35. Pfurtscheller, G., & Lopes da Silva, F. H. (1999). Event-related EEG/MEG synchronization and desynchronization: Basic principles. *Clinical Neurophysiology*, *110*(11), 1842–1857. https://doi.org/10.1016/S1388-2457(99)00141-8

36. Picton, T. W., Bentin, S., Berg, P., Donchin, E., Hillyard, S. A., Johnson, R., Miller, G. A., Ritter, W., Ruchkin, D. S., Rugg, M. D., & Taylor, M. J. (2000). Guidelines for using human event-related potentials to study cognition: Recording standards and publication criteria. *Psychophysiology*, *37*(2), 127–152. https://doi.org/10.1111/1469-8986.3720127

37. Pouget, P., Allard, E., Poitou, T., Raux, M., Wattiez, N., & Similowski, T. (2018). Slower Is Higher: Threshold Modulation of Cortical Activity in Voluntary Control of Breathing Initiation. *Frontiers in Neuroscience*, *12*. https://www.frontiersin.org/articles/10.3389/fnins.2018.00663

38. Provost, A., Jamadar, S., Heathcote, A., Brown, S. D., & Karayanidis, F. (2018). Intertrial RT variability affects level of target-related interference in cued task switching. *Psychophysiology*, *55*(3). Scopus. https://doi.org/10.1111/psyp.12971

39. Raux, M., Navarro-Sune, X., Wattiez, N., Kindler, F., Le Corre, M., Decavele, M., Demiri, S., Demoule, A., Chavez, M., & Similowski, T. (2019). Adjusting ventilator settings to relieve dyspnoea modifies brain activity in critically ill patients: An electroencephalogram pilot study. *Scientific Reports*, *9*(1), 16572. https://doi.org/10.1038/s41598-019-53152-y

40. Raux, M., Straus, C., Redolfi, S., Morelot-Panzini, C., Couturier, A., Hug, F., & Similowski, T. (2007). Electroencephalographic evidence for pre-motor cortex activation during inspiratory loading in humans. *The Journal of Physiology*, *578*(Pt 2), 569–578. https://doi.org/10.1113/jphysiol.2006.120246

41. Smith, S. M., & Nichols, T. E. (2009). Threshold-free cluster enhancement: Addressing problems of smoothing, threshold dependence and localisation in cluster inference. *NeuroImage*, *44*(1), 83–98. https://doi.org/10.1016/j.neuroimage.2008.03.061

42. Straus, C., Locher, C., Zelter, M., Derenne, J.-P., & Similowski, T. (2004). Facilitation of the diaphragm response to transcranial magnetic stimulation by increases in human respiratory drive. *Journal of Applied Physiology (Bethesda, Md.: 1985)*, *97*(3), 902–912. https://doi.org/10.1152/japplphysiol.00989.2003

43. Tallon-Baudry, C., & Bertrand, O. (1999). Oscillatory gamma activity in humans and its role in object representation. *Trends in Cognitive Sciences*, *3*(4), 151–162. https://doi.org/10.1016/S1364-6613(99)01299-1

44. Tremoureux, L., Raux, M., Hudson, A. L., Ranohavimparany, A., Straus, C., & Similowski, T. (2014). Does the supplementary motor area keep patients with Ondine's curse syndrome breathing while awake? *PLoS One*, *9*(1), e84534. https://journals.plos.org/plosone/article?id=10.1371/journal.pone.0084534

45. van den Bosch, O. F. C., Alvarez-Jimenez, R., de Grooth, H.-J., Girbes, A. R. J., & Loer, S. A. (2021). Breathing variability-implications for anaesthesiology and intensive care. *Critical Care (London, England)*, *25*(1), 280. https://doi.org/10.1186/s13054-021-03716-0

46. Wagner, J., Martínez-Cancino, R., & Makeig, S. (2019). Trial-by-trial source-resolved EEG responses to gait task challenges predict subsequent step adaptation. *NeuroImage*, *199*, 691–703. https://doi.org/10.1016/j.neuroimage.2019.06.018

47. Wang, Y., Veluvolu, K. C., Cho, J.-H., & Defoort, M. (2012). Adaptive estimation of EEG for subject-specific reactive band identification and improved ERD detection. *Neuroscience Letters*, *528*(2), 137–142. https://doi.org/10.1016/j.neulet.2012.09.001

48. Watanabe, T., Itagaki, A., Hashizume, A., Takahashi, A., Ishizaka, R., & Ozaki, I. (2023). Observation of respiration-entrained brain oscillations with scalp EEG. *Neuroscience Letters*, *797*, 137079. https://doi.org/10.1016/j.neulet.2023.137079